In Vivo Measurement of Rat Brain Water Content at 9.4 T MR Using Super-Resolution Reconstruction: Validation With Ex Vivo Experiments

Dennis C. Thomas, MMST,^{1,2} Ana-Maria Oros-Peusquens, PhD,^{1*} Michael Schöneck, MSc,¹ Antje Willuweit, PhD,¹ Zaheer Abbas, PhD,¹ Markus Zimmermann, PhD,¹ Jörg Felder, PhD,^{1,3} Avdo Celik, MSc,⁴ and Nadim Joni Shah, PhD^{1,4,5,6}

Background: Given that changes in brain water content are often correlated with disease, investigating water content non-invasively and in vivo could lead to a better understanding of the pathogenesis of several neurologic diseases.

Purpose: To adapt a super-resolution-based technique, previously developed for humans, to the rat brain and report in vivo high-resolution (HR) water content maps in comparison with ex vivo wet/dry methods.

Study Type: Prospective.

Animal Model: Eight healthy male Wistar rats.

Field Strength/Sequence: 9.4-T, multi-echo gradient-echo (mGRE) sequence.

Assessment: Using super-resolution reconstruction (SRR), a HR mGRE image (200 µm isotropic) was reconstructed from three low-resolution (LR) orthogonal whole-brain images in each animal, which was followed by water content mapping in vivo. The animals were subsequently sacrificed, the brains excised and divided into five regions (front left, front right, middle left, middle right, and cerebellum-brainstem regions), and the water content was measured ex vivo using wet/dry measurements as the reference standard. The water content values of the in vivo and ex vivo methods were then compared for the whole brain and also for the different regions separately.

Statistical Tests: Friedman's non-parametric test was used to test difference between the five regions, and Pearson's correlation coefficient was used for correlation between in vivo and ex vivo measurements. A *P*-value <0.05 was considered statistically significant.

Results: Water content values derived from in vivo MR measurements showed strong correlations with water content measured ex vivo at a regional level (r = 0.902). Different brain regions showed significantly different water content values. Water content values were highest in the frontal brain, followed by the midbrain, and lowest in the cerebellum and brainstem regions.

Data Conclusion: An in vivo technique to achieve HR isotropic water content maps in the rat brain using SRR was adopted in this study. The MRI-derived water content values obtained using the technique showed strong correlations with water content values obtained using ex vivo wet/dry methods.

Level of Evidence: 1 Technical Efficacy: Stage 1

J. MAGN. RESON. IMAGING 2024;60:161-172.

View this article online at wileyonlinelibrary.com. DOI: 10.1002/jmri.29061

Received May 25, 2022, Accepted for publication Sep 29, 2023.

*Address reprint requests to: A.-M.O.-P., Institute of Neuroscience and Medicine 4, INM-4, Forschungszentrum Jülich, Leo-Brandt-Str, 52428 Jülich, Germany. E-mail: a.m.oros-peusquens@fz-juelich.de

Dennis C. Thomas and Ana-Maria Oros-Peusquens are joint first authors.

From the ¹Institute of Neuroscience and Medicine 4, INM-4, Forschungszentrum Jülich, Jülich, Germany; ²Faculty of Medicine, RWTH Aachen University, Aachen, Germany; ³RWTH Aachen University, Aachen, Germany; ⁴Institute of Neuroscience and Medicine 11, INM-11, JARA, Forschungszentrum Jülich, Jülich, Germany; ⁵JARA—BRAIN—Translational Medicine, Aachen, Germany; and ⁶Department of Neurology, RWTH Aachen University, Aachen, Germany

Additional supporting information may be found in the online version of this article

This is an open access article under the terms of the Creative Commons Attribution-NonCommercial-NoDerivs License, which permits use and distribution in any medium, provided the original work is properly cited, the use is non-commercial and no modifications or adaptations are made.

nimal disease models are an important tool for widening Aour understanding of the pathogenesis and longitudinal evolution of brain diseases. Rat models for stroke, traumatic brain injury (TBI), Parkinson's disease, and Alzheimer's disease are well established. 1-5 Water content is known to be well regulated in the brain and is expected to change in almost all brain disorders.⁶ For example, ischemia, brain injuries, and hypoxia in the brain are all associated with changes in water content in humans.⁷⁻¹¹ Furthermore, total water content is often found to be increased in patients with tumors or multiple sclerosis (MS). 12-15 Using ex vivo techniques, some studies have characterized the water content of the normal rat brain, 16-18 while other studies have investigated the changes in water content in different disease states like ischemia, hypertension, space-occupying lesions, arterial hypertension, and water intoxication. $^{10,19-21}$ Since the water content is known to be tightly regulated in the healthy brain and since water content is very sensitive to pathologies in the brain, it is indeed desirable to develop a robust method to non-invasively measure the water content of the brain in rats. Wet/dry methods are considered the reference standard for ex vivo water content measurements. 16,18 However, given that this invasive method cannot be performed in vivo, it cannot be applied in patient diagnostics and can only serve as a research tool. In contrast, MRI offers a non-invasive way to study in vivo changes in the brain following the onset of disease. In this context, studies with animal models could be useful for the purpose of validating MRI techniques following the sacrifice of the animals, and the ex vivo brain can be used to correlate the changes seen in MRI to those seen on histological sections of the rat brain. Quantitative validation of MRI-based measurements offers the opportunity to transfer new methods to human applications, providing potential for further research and diagnosis. Based on initial research using ex vivo techniques in animals, over the past three decades, MRI techniques to map the water content of the in vivo human brain have been developed. 22-26 With ever-increasing access to MRI in the clinical context, it can be expected that quantitative MRI (qMRI)-based water content measurement will gain a role in the clinical routine for the evaluation of patients with diseases such as MS, Alzheimer's disease, hepatic encephalopathy, and brain tumors.

To date, only a few studies have tried to validate animal brain water content obtained by MRI against the reference standard of ex vivo wet/dry techniques. Lin et al validated their water content mapping technique using a 3-T small animal MRI scanner in Long Evans rats with focal cerebral ischemia. However, the water content mapping technique employed required corrections for T_1 bias in the fast low-angle shot (FLASH) images, resulting in the need for additional scan time. Using a similar method, Schwarcz et al attempted to carry out water content mapping at 9.4 T in mice with induced vasogenic edema. However, a critical

assessment of the accuracy of the water content values obtained was not carried out.²⁸ No further study that correlated the MRI-based water content mapping techniques with wet/dry ex vivo techniques has been conducted, despite a number of advances in water content mapping techniques. Of particular note are the robust corrections made for the bias caused due to differing T₁ and T₂* decay and the B₁ field inhomogeneities in different regions of the brain. 22,23,30 Furthermore, previous techniques used an external water phantom to achieve calibration, requiring additional corrections for the difference between the phantom and rat body temperature. Although used in a similar manner in humans at lower fields, 22 at higher fields, this calibration method has been replaced with the use of cerebrospinal fluid (CSF) as the internal calibration standard for 100 p.u. (percentage units) water. 24,26,30 Recently, a single-scan technique has been developed that avoids the need for additional scans for T₁ correction, thus decreasing scan time and improving clinical applicability.²⁴ A high signal-to-noise ratio (SNR) is crucial for accurate qMRI mapping, and super-resolution reconstruction (SRR) techniques can provide a further advantage in the trade-off between SNR, acquisition time, and resolution.³¹ Recently, SRR techniques were combined with a modified version of the single-scan water content mapping technique²⁴ to obtain accurate water content maps of the in vivo human brain at isotropic high resolution (HR). 32,33 The biggest hurdle in obtaining accurate water content maps—especially at very high field strengths—is the presence of radiofrequency (RF) magnetic field inhomogeneities in the MRI data. This is because the receive field B_1^- (or sensitivity) is difficult to measure accurately in vivo. Similar to the transmit field B₁⁺, B₁⁻ is modified by interactions with the sample placed inside the coil and hence is different for every subject.

Against this background, we aimed to compare the water content values obtained in five regions (front left, front right, middle left, middle right, and the cerebellum-brainstem regions [CB-BS]) using a proposed super-resolution-based in vivo MRI technique with bias field correction to those obtained with ex vivo wet/dry methods as the reference standard. We further aimed to investigate the observed broad regional variations in the water content of the rat brain.

Materials and Methods

All animals were handled in accordance with the guidelines of the Animal Research Committee of our institute. The local ethics committee approved this prospective study.

Animals

Experiments were carried out on a total of eight male Wistar rats (Charles River Laboratories, Sulzfeld, Germany), with an age range of 10–11 weeks and a mean weight of 400 g. All rats were housed in groups of at least two under standard conditions. Food and water were provided ad libitum.

Thomas et al.: In Vivo Measurement of Rat Brain Water Content

In Vivo MRI Methods

DATA ACQUISITION AND SRR RECONSTRUCTION. The rats were first scanned with a 9.4-T MRI scanner and later sacrificed to carry out the ex vivo studies. The MRI experiments were carried out in an in-house assembled small animal 9.4-T MRI scanner. 34 A body coil was used for RF transmission, and a four-channel phased array receive coil (Rapid Biomedical, Rimpar, Germany) was used for receiving the signal. For animal supervision, the acquisitions of electrocardiography (ECG), respiration rate, and temperature were carried out using a commercially available monitoring system (Small Animal Instruments Inc., Stony Brook, NY, USA). The monitoring system provides a user-configurable respiration trigger signal that is interfaced with the MRI scanner to enable synchronized sequences using the breathing signals of the animal. In the method described previously, three orthogonal low-resolution (LR) multi-echo gradient echo (mGRE) images were acquired and recombined using SRR to obtain a single HR mGRE image, which was then used for water content mapping.³² Similarly, three orthogonally oriented LR mGRE images (12 echoes) with an in-plane resolution of $200 \ \mu m \times 200 \ \mu m$ and a slice thickness of 600 μm were acquired. The sequence parameters were as follows: repetition time (TR) flip angle $(FA) = 15^{\circ}$, = 3330 msec,first echo $(TE)_0 = 1.35$ msec, $\Delta TE = 2.10$ msec, nTE (number of echoes) bandwidth = 650 Hz/pixel, field of view $= 38.4 \text{ mm} \times 38.4 \text{ mm},$ matrix size = 192×192 , partial Fourier = 6/8, no. of slices = 90, and 4 averages per orientation. The total measurement time was 2 hours. The four datasets acquired for each orientation were averaged to obtain three high SNR and orthogonally oriented LR mGRE images. These were then SRR recombined to obtain one HR mGRE image (12 echoes) of isotropic voxel size of 200 µm cubic, as shown in Fig. 1. The SNR was calculated by taking the average intensity of an ROI in the corpus callosum at the midline and dividing it by the SD of an ROI selected right outside the rat brain area.

SRR THEORY. The three high SNR and orthogonally oriented LR mGRE magnitude images can be denoted as LR₁, LR₂, and LR₃. Each of these images had a resolution of 200 μ m \times 200 μ m \times 600 μ m. It is possible to reconstruct one HR mGRE image (200 μ m \times 200 μ m \times 200 μ m) with $O(3 \cdot m \times 1)$ as the vector of the HR object that we aimed to reconstruct, where m is the number of voxels in the individual LR images. The acquisition of LR $_i$ ($j=1 \dots 3$) can then be modeled as follows:

$$LR_i = X_i O + e_i, \tag{1}$$

where $e_j(m\times 1)$ represents the noise corresponding to the jth LR image, and $X_j(m\times 3\cdot m)$ is the transformation matrix that maps O to the jth LR image. The acquisition of the vector $S(3\cdot m\times 1)$, containing all LR image voxels from the LR images, can then be modeled as follows:

$$S = XO + e, \tag{2}$$

with

$$S = \begin{bmatrix} LR_1 \\ LR_2 \\ LR_3 \end{bmatrix}, X = \begin{bmatrix} X_1 \\ X_2 \\ X_3 \end{bmatrix}, e = \begin{bmatrix} e_1 \\ e_2 \\ e_3 \end{bmatrix}.$$
 (3)

The problem of estimating O is then reduced to a minimization problem of finding the optimum O such that the squared difference between the predicted LR images and the actual LR images is minimized. L2-based (Laplacian) regularization is added to improve robustness, leading to the following regularized linear least-squares problem:

$$\arg \min_{O} ||XO - S||_{2}^{2} + \lambda ||TO||_{2}^{2},$$

where T computes the squared partial second derivates of O along the x-, y-, and z-directions and λ is the regularization value. This regularized least-squares problem was solved efficiently using a method described previously, based on the conjugate-gradient method.³⁵ The λ value used depends on the SNR of the first TE image of the individual LR images. In this work, the SNR of the first echo of the individual LR images was \sim 100. Hence, a relatively low regularization value of 0.05 was used for SRR of all datasets. Figure S1 in the Supplemental Material shows the effect of λ value on the reconstructed water content maps. An optimum λ value of 0.05 gives a good trade-off between increased noise (low λ value) and increased blurring (high λ value). Apart from the final resolution of the SRR mGRE image and the regularization used, the SRR reconstruction framework used in this work is exactly the same as that used in Ref. 33. In Eq. 3, LR1, LR2, and LR3 were vectorized in such a way that the voxels from the different echoes were concatenated one after the other to obtain 3 1D vectors for each of the LR images. The matrix X was constructed by constructing the implicit matrix as described by Poot et al and replicating it for 4D mGRE, as is currently the case.³⁵

WATER CONTENT MAPPING. The reconstructed 12-echoes HR mGRE image was then used to perform water content mapping using CSF as an internal 100 p.u. water reference. The method used for water content mapping was similar to that described previously.³³ In Ref. 33, the HR mGRE image was corrected for B₁⁺ and B₁⁻ field (receive field) inhomogeneities and T₂* relaxation to obtain the M0 map. The final H_2O map was obtained by dividing the M0map by a calibration factor. The calibration factor was calculated from the M0 values of the CSF voxels, corrected for a saturation factor of 0.97 for the incomplete T1 recovery of the CSF voxels. However, a few notable differences were required in three preprocessing steps in order to adapt the method to animal imaging and an ultra-high field strength: 1) receive field inhomogeneity correction, 2) CSF mask generation, and 3) T2* correction. These modifications are described in detail below. In order to properly evaluate the advantages of employing SRR, water content maps were obtained using the SRR HR image (SRR-H2O) and also using the three individual LR mGRE datasets (LR-H2O).

Receive field inhomogeneity correction. First, the brain masks were generated manually by D.C.T. with 4 years of experience in animal and human brain MRI imaging, using ITK SNAP (version

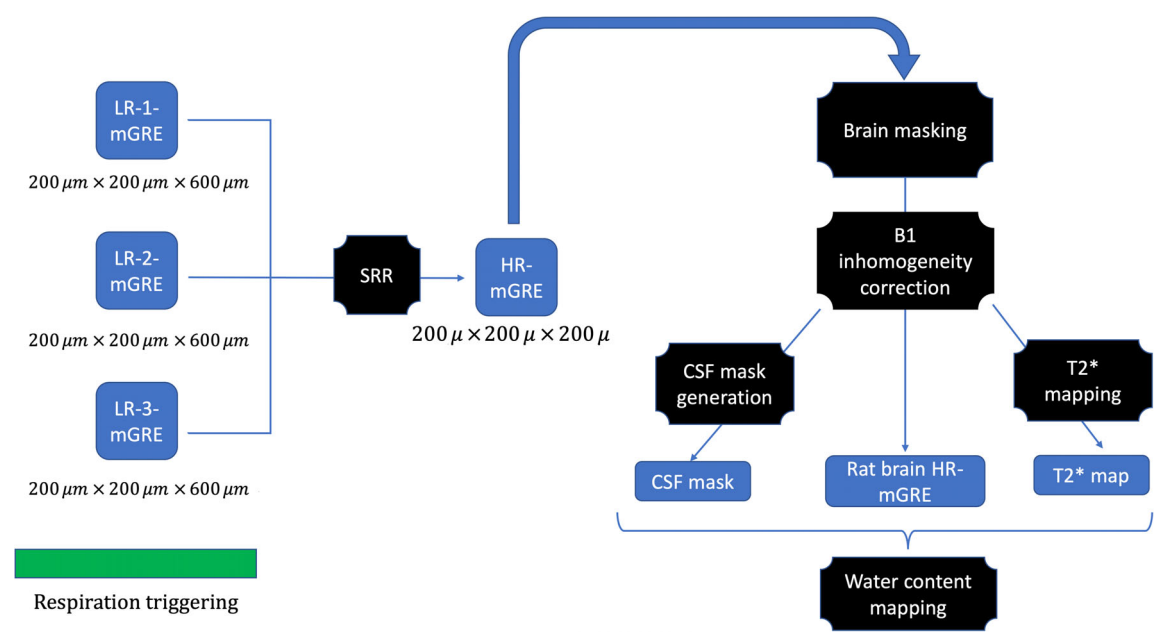


FIGURE 1: Schematic showing the steps of data acquisition, image reconstruction, and the data processing pipeline.

3.8.0; http://www.itksnap.org/pmwiki/pmwiki.php).³⁶ The whole brain was segmented out for each rat and care was taken to include the CSF voxels surrounding the rat brain in the brain mask. The skull-stripped HR mGRE images were then corrected for the receive field inhomogeneities using the N4 bias field correction algorithm.³⁷ The bias field was estimated using the first echo (high SNR) image. The default parameters with were used for the latter, the number iterations = $100 \times 100 \times 100 \times 100$. Additionally, the brain mask was provided as the "mask" so that the bias field algorithm only corrected for the bias field in the brain region. The estimated bias field from the first echo image was used to correct all the echoes for the receive field inhomogeneity.

CSF mask generation. The pixel intensities (PIs) of the first echo of the bias-field-corrected HR mGRE images were sorted in ascending order (bold black line in the graph in Fig. 2). Due to the presence of numerous structures in the brain with different water content values, and because of the presence of partial volume effects in the bordering voxels in these structures, the MRI-based water content can be expected to increase smoothly and linearly in the middle portion of the curve. Hence, the middle 1,000,000 pixels were fitted with a straight line (bold green line in the graph in Fig. 2). This linear fit was then extrapolated (dashed green line). When denoting the mean pixel intensity as *I*, all pixels with a difference between the normalized pixel intensity (normalized to *I*) and the linear fit greater than a predefined threshold value (*k*) were considered as belonging to the CSF.

$$CSF mask = \begin{cases} 1, & (PI/I - (mx + c)) > k \\ 0, & \text{otherwise} \end{cases}, \tag{4}$$

where (mx+c) is the linear fit and k is a predefined threshold value. The value of k was empirically set to a conservative value of 0.095, thus excluding the CSF voxels affected by partial volume effects and only including the "pure" CSF voxels. For the CSF calibration in

the LR-based water content mapping, the value of k was determined empirically and was set to 0.030 for all LR datasets. Figure S2 in the Supplemental Material shows the effect of k-value on the CSF mask generated for TRA-H₂O.

 T_2* correction, M_0 calculation, and calibration. The bias-field-corrected HR mGRE images were used to perform a voxel-wise mono-exponential fit of the T_2* decay. Due to the high B_0 field, the T_2* values for the brain tissue were found to be shorter (\sim 25 msec) than at 3 T (\sim 50 msec). The T_2* values for the brain tissue were found to lie between 15 msec and 45 msec. Further, ROIs were defined in the corpus callosum and in the cortex adjacent to the corpus callosum for one of the rats. The mean T_2* values in these regions were analyzed. The T_2* maps obtained were then used to perform voxel-wise extrapolation of the first echo to TE=0:

$$M_0 = \frac{S(\text{TE}_1)}{e^{-\text{T}_2} / \text{TE}_1}$$
 (5)

The correction in Eq. 5 was only performed for voxels with 15 msec < $T_2* <$ 45 msec. Voxels with $T_2* >$ 45 msec were considered to belong to the CSF. T_2* correction was not carried out in these voxels since the T_2* fitting was not robust. It was assumed that the CSF signal did not decay between TE=0 msec and TE=1.35 msec (first TE). The final water content maps were obtained by CSF calibration from M_0 , as reported previously.³²

Ex Vivo Wet/Dry Measurements

Following the MRI experiments, the rats were sacrificed in deep inhalation anesthesia using a guillotine. The brain was excised and divided into five regions as follows: frontal left (FL), frontal right (FR), midbrain left (ML), midbrain right (MR), and the CB–BS regions as shown in Fig. 3. The CB–BS was dissected out first from the rest of the brain by cutting along the groove separating the CB–BS from the cerebral hemispheres. Then, the olfactory lobes

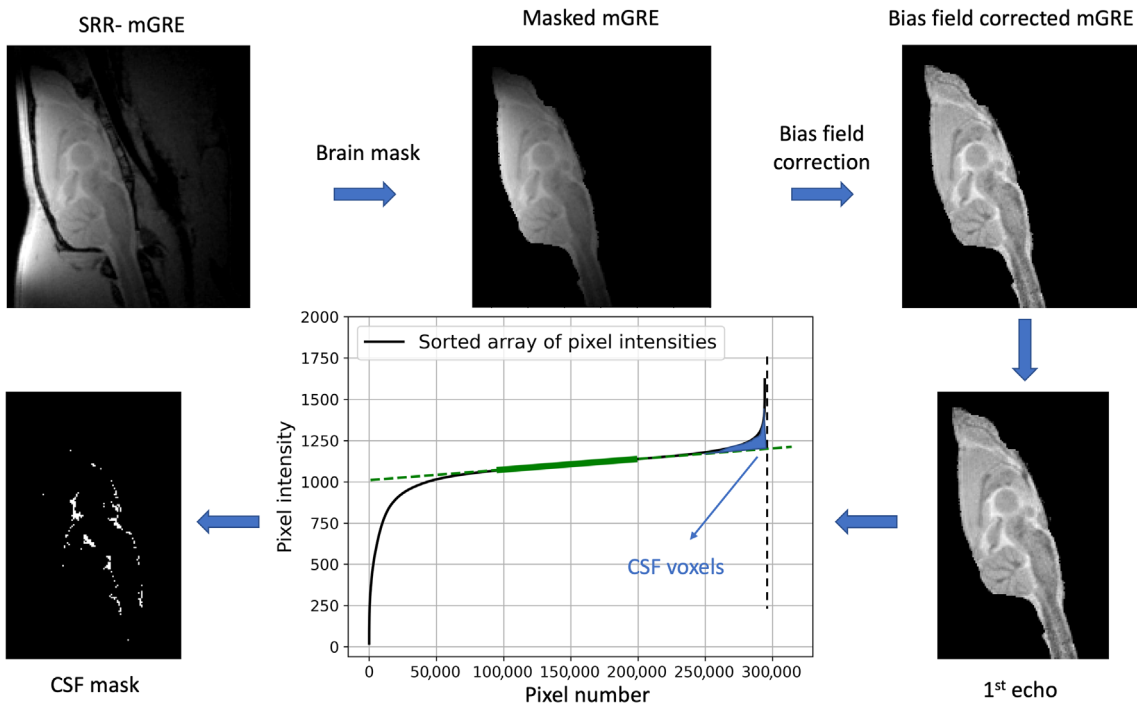


FIGURE 2: The pipeline for brain masking, bias field correction, and CSF mask generation is shown here. The images in the bottom row show the generation of the CSF mask. The bold black line in the graph shows the sorted array of pixel intensities for the first echo of the bias field corrected mGRE image. The bold green line is the linear fit of the middle 1,000,000 pixels. The area shaded in blue represents the CSF voxels. In the graph, the pixel numbers are ordered in ascending intensity from left to right.

were removed. The length of the cerebral hemispheres was measured and a line was marked at the midline of the length of the cerebral hemispheres. A cut was made at this line to separate the Frontal from the midbrain region. The right and left frontal and midbrain regions were then separated by an incision along the interhemispheric fissure.

For all animals, the five tissue samples were then weighed immediately on a basic precision measuring scale (KERN ABJ-NM [Kern & Sohn GMBH, Balingen, Baden-Wüttemberg, Germany], precision = 0.1 mg) and placed into an oven that had been preheated to 72 °C. The tissue samples were dried in the oven for up to 42 hours at 72 °C. The tissue samples were weighed intermittently to track the evaporated percentage of water. The weight was found to remain constant after a period of 35 hours. To be on the safer side, we chose 42 hours as the time to completely dry the

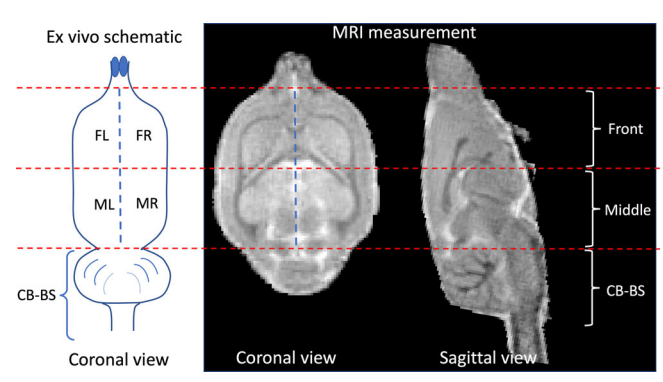


FIGURE 3: Figure depicting the division of the ex vivo brain and the in vivo MR brain images into the five regions.

tissue. The weight measured after 42 hours was used to calculate the water content of each of the tissue samples as follows:

Water content [p.u.] =
$$\frac{\text{wet weight} - \text{dry weight (at 42 hours)}}{\text{wet weight}}$$
$$\times 100.$$
 (6)

Data Analysis: Comparison of In Vivo and Ex Vivo Measurements

The water content maps were obtained for all rats as described above and regionally compared to the ex vivo information. The in vivo water content maps were also divided into the five regions as shown in Fig. 3. The olfactory lobes were excluded as these were cut out in the ex vivo experiments. To divide the brain into the front, middle, and CB-BS regions, the sagittal orientation of the MRI data was used. The superior border of the cerebellum was used to delineate the separation between the CB-BS regions and the rest of the brain. The rest of the brain was then divided into the front and middle regions by dividing the remaining brain into two equal halves. For the division of the front and middle regions into front-left, front-right, middle-left, and middle-right, the coronal orientation was used. An upper limit of 86 p.u. was selected to completely exclude all voxels belonging to CSF and also white matter (WM) and gray matter (GM) voxels bordering CSF spaces, which might be affected by partial volume effects. Also, the water content of all brain regions in Wistar rats was below 86 p.u., as reported earlier. 16 The mean in vivo water content of the whole brain was compared with the mean ex vivo water content of the whole brain, calculated as a weighted mean:

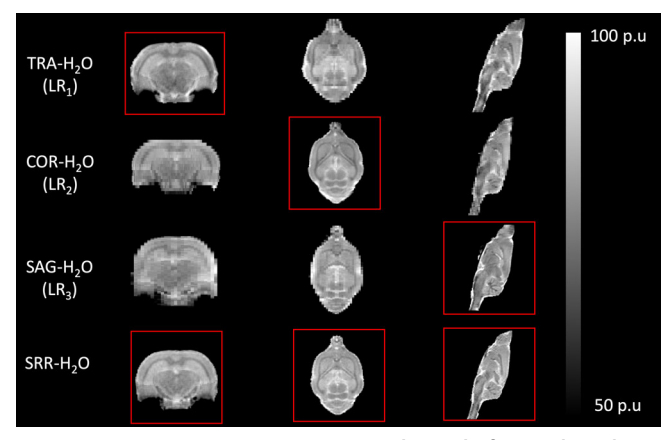


FIGURE 4: Water content maps derived from the three orthogonal LR images (TRA: transverse, COR: coronal, SAG: sagittal) and from the SRR-H₂O method of a representative animal. The red box denotes the high-resolution plane (in-plane). As is seen, the SRR-H₂O water content maps have a high resolution in all three orientations.

Whole brain
$$H_2O = \frac{\sum\limits_{i=1}^{5} H_2O(i) \times \text{wet weight}(i)}{\sum\limits_{i=1}^{5} \text{wet weight}(i)},$$
 (7)

where i = 1, 2, 3, 4, 5 refers to the different tissue samples FL, FR, ML, MR, and CB-BS, respectively.

Statistical Analysis

Statistical evaluation was performed using Python (version 3.7; https://www.python.org/, Scipy and Numpy packages). Comparisons of the different brain regions (FL, FR, ML, MR, and CB-BS) were made using a non-parametric Friedman's test. A Pearson's correlation analysis was done for correlations between data resulting from ex vivo and in vivo measurements both at a whole brain level and at a regional level. Box plots were generated for the data of this study

where applicable, including the median and mean values and interquartile ranges or SD, as well as minimum and maximum values. A P-value of <0.05 was considered statistically significant.

Results

In Vivo Results

Figure 4 shows the water content maps obtained using both the individual LR images and the SRR-H₂O method. It can be seen that SRR-H₂O produced high and isotropic water content maps, while the individual LR-H₂O maps had a high in-plane but a lower through-plane resolution. Figure 5 shows one of the in vivo water content maps in the three orthogonal orientations with an isotropic voxel size (200 µm). Qualitatively, it can be seen that the low-frequency variation of intensity (as a result of receive field inhomogeneities) was well corrected. Furthermore, good contrast was achieved between WM, GM, and CSF. The mean whole-brain water content value for this particular rat was 77.43 p.u. The water content in the different brain regions ranged from 71 p.u. to 85 p.u.

At the group level, the whole-brain water content was found to be 77.48 \pm 0.33 p.u. (mean \pm SD). Figure 6 shows the T2* maps for the same rat brain obtained with a monoexponential fit of the mGRE decay curve, and it can be seen that the T₂* maps also provided good contrast between WM and GM. The T₂* values of the different brain regions varied from 15 msec to 45 msec. In a region of interest (ROI) selected in the corpus callosum, the T₂* value was found to be 22.6 ± 2.0 msec. In an ROI in the cortex right adjacent to the corpus callosum ROI, the T2* values were found to be 39.96 ± 3.03 msec. Since the bony (air-filled) part of the ear canals is quite large in rats, the areas near the ear canals are prone to strong B₀ inhomogeneity artifacts, which can lead to a rapid decay of the T₂* signal. This leads to abnormally low T₂* values near the ear canals, as seen by the red arrows shown in Figure 6.

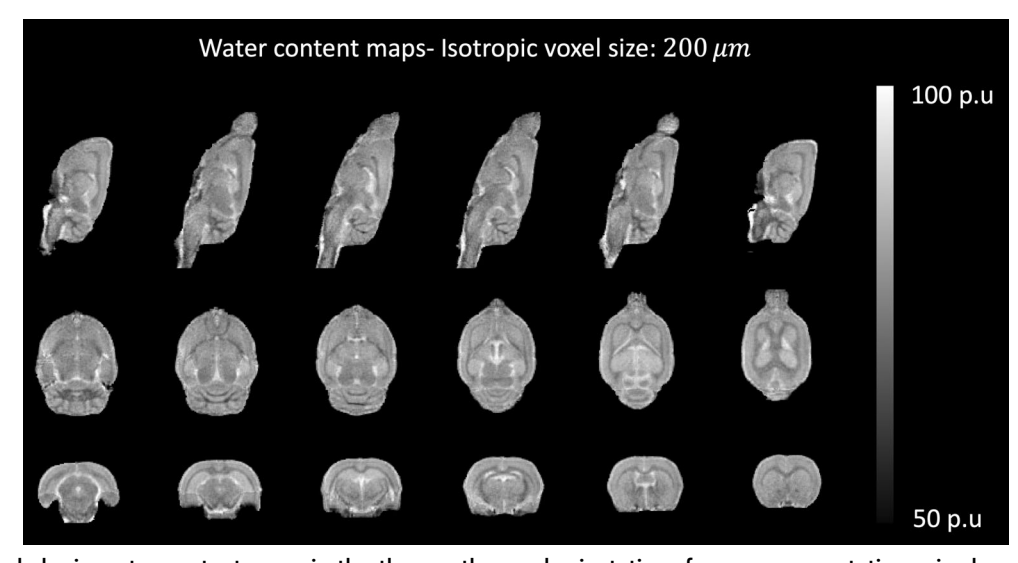


FIGURE 5: Whole-brain water content maps in the three orthogonal orientations from a representative animal: sagittal (top row), coronal (middle row), and axial (bottom row) views.

FIGURE 6: Whole-brain T_2^* maps in the three orthogonal orientations for the same rat brain shown in Fig. 4. The red arrows show the areas which are affected by strong B_0 inhomogeneity effects. These regions are close to the bony auditory canal.

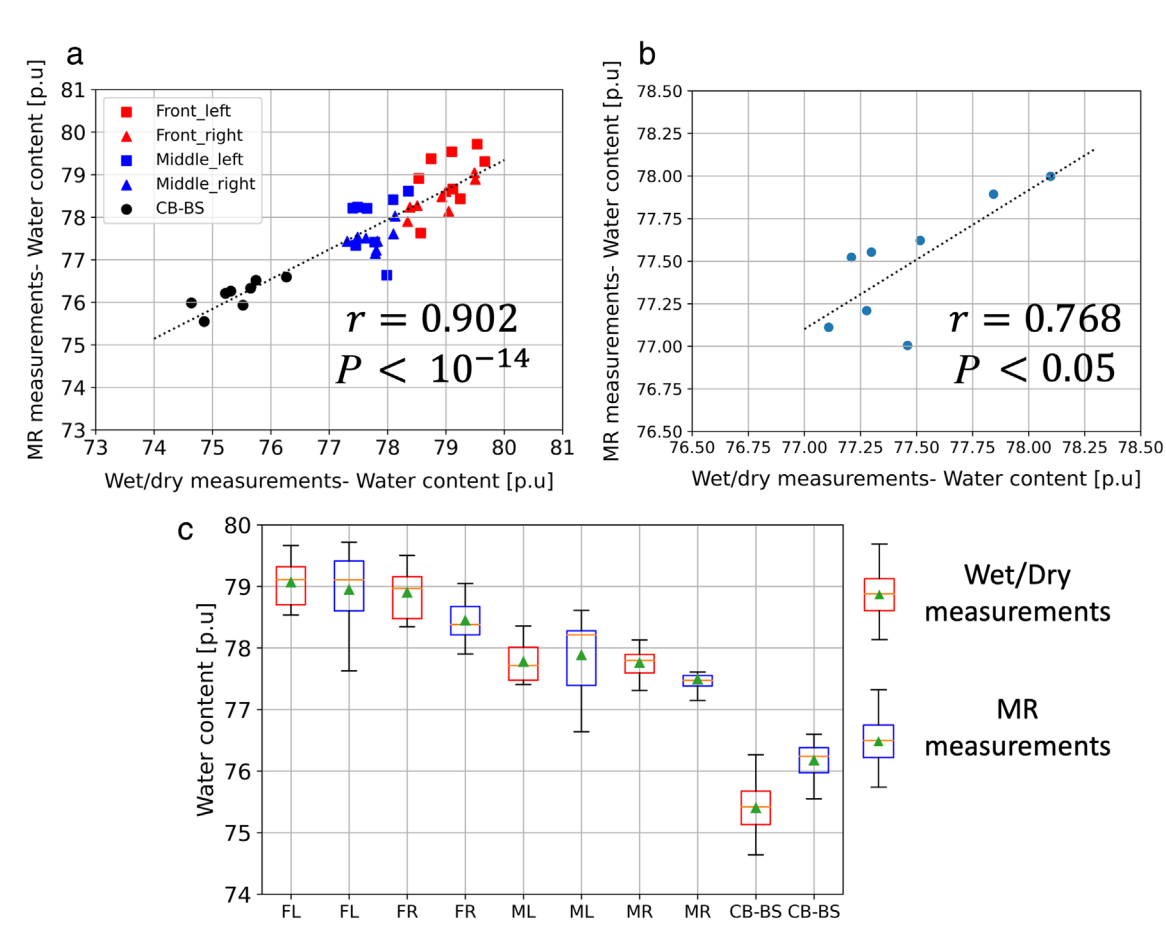


FIGURE 7: (a) Correlation between the water content values obtained with MR measurements and those obtained with wet/dry measurements at a regional level (linear fit: y = 0.70x + 23.39). (b) Correlation at the whole-brain level (linear fit: y = 0.81x + 14.29). (c) Box plots of the water content values of the five brain tissue samples as measured ex vivo using wet/dry measurements. FL = front left; FR = front right; ML = middle left; MR = middle right; CB-BS = cerebellum-brainstem. In each box plot, the orange line represents the median, the green arrow shows the mean value, the box represents the interquartile range, and the whiskers represent the minimum and maximum value of the water content values of the eight rats.

July 2024 167

A good and significant correlation (0.76) between the SRR-H₂O and wet/dry measurements is evident in Figure 7. As seen in the Bland–Altman plots shown in Figure 8, the bias is relatively low for the SRR-H₂Os and LR-H₂Os. However, SRR-H₂O has the least bias (-0.01 p.u.) followed by TRA-H₂O (-0.13 p.u.), SAG-H₂O (0.95 p.u.) and COR-H₂O (0.98 p.u.). Further SRR-H₂O also has the lowest 1.96 SD limits [0.42, -0.45]. The Bland–Altman plots show a very good agreement between SRR-H₂O and the reference wet/dry measurements.

Figure 9a shows the T_2^* maps of a representative rat brain dataset using the LR datasets and the SRR-reconstructed HR image. No clear differences were apparent in the distribution of T_2^* values in the brain. Figure 9b shows the histogram of the whole-brain T_2^* values for each individual LR acquisition and the SRR. The distribution of the values within the histograms was also similar. For further exemplification of this point, the T_2^* maps are compared between TRA- T_2^* and SRR- T_2^* in Fig. 9c. The mean T_2^* values in the ROI delineated in the corpus callosum were 23.04 ± 3.28 (TRA- T_2^*) and 24.74 ± 3.95 (SRR- T_2^*).

Figure S3 in the Supplemental Material shows the comparison between the CSF masks obtained using the SRR-H₂O method and the three LR-H₂O methods. It can be noticed that the CSF masks obtained using the SRR-H₂O method lead to selection of fewer voxels with partial volume

effects as opposed to the CSF masks obtained using the LR images. Correspondingly, the SRR-H₂O method could lead to a more conservative delineation of the CSF voxels, thus only the pure CSF voxels could be selected. This possibly leads to a higher accuracy of the water content values obtained using the SRR-H₂O method.

Ex Vivo Results

The ex vivo water content results showed some regional dependence. The water content values of FL and FR converged at ~78.50 p.u., the water content values of ML and MR converged at \sim 77.50 p.u., and the water content value of the CB-BS regions converged at 75.28 p.u. At a group level, the water content values of all rat brains measured with the wet/dry method appeared to be similar in both hemispheres, but differed between regions (Fig. 7). The water content values between the front (FL/FR), middle (ML/MR), and CB-BS regions were significantly different (Table 1). No significant difference was observed between the water content values between the left and right hemispheres. The wholebrain ex vivo water content at the group level was found to be 77.47 \pm 0.31 p.u. (mean \pm SD). The whole brain water content values measured using the wet/dry agreed with values previously reported in the literature (mean values ranging from 76.08 p.u. to 80.1 p.u.). 11,20,27,38

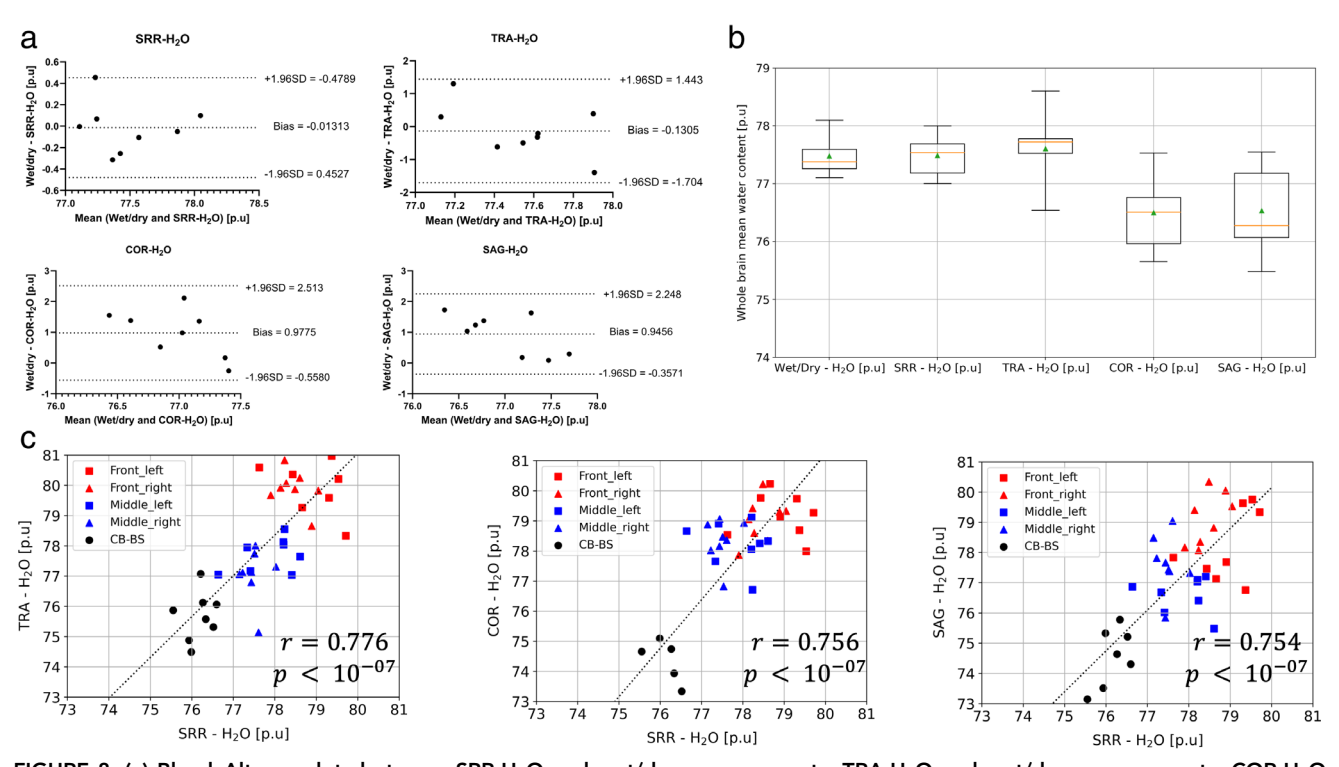


FIGURE 8: (a) Bland–Altman plots between SRR-H₂O and wet/dry measurements, TRA-H₂O and wet/dry measurements, COR-H₂O and wet/dry measurements, and SAG-H₂O and wet/dry measurements. (b) Box plots comparing the whole brain mean water content values with the different methods. In each box plot, the orange line represents the median, the green arrow shows the mean value, the box represents the interquartile range, and the whiskers represent the minimum and maximum value of the water content values of the eight rats. (c) Correlations between SRR-H₂O and the individual LR-H₂Os.

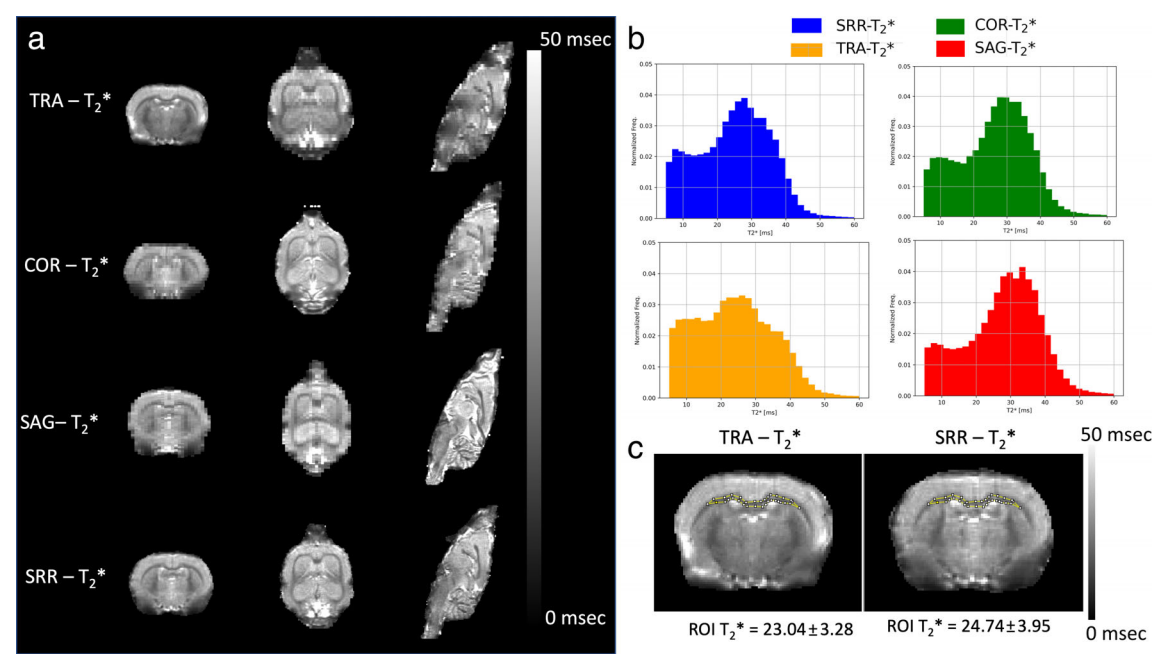


FIGURE 9: (a) T_2^* maps obtained using the SRR-HR image (SRR- T_2^*) and using the individual LR images (TRA- T_2^* , COR- T_2^* , and SAG- T_2^*). (b) Histograms of the T_2^* values (15 msec < T_2^* < 45 msec) obtained with the SRR- H_2^* O method and the LR- H_2^* O methods. (c) ROI-based comparison of the T_2^* values from T_2^* maps obtained using the SRR-HR image and the TRA-LR image. The ROI is selected in the region of the corpus callosum (CC).

Correlation and Comparison of Water Content Measured In Vivo and Ex Vivo

The water content values of the different regions obtained with the MRI experiments and with the reference standard of ex vivo wet/dry measurements are shown in Table 1. The SD of the SRR- H_2O (0.33 p.u.) was found to be comparable with that of the ex vivo measurements (0.31 p.u.). Figure 7 shows the correlation between water content values obtained using MRI measurements and wet/dry measurements. A strong correlation was achieved between the water content values in the different brain regions obtained with the ex vivo and in vivo methods (r = 0.902; Fig. 7a). At the whole-brain level, a good correlation between the MR measurements and wet/dry measurements was noted with a Pearson's correlation coefficient r = 0.768 (Fig. 7b). With the wet/dry measurements, the whole-brain water content values had a narrow range from 77.20 to 78.20 p.u. Even within this

narrow range, a good correlation between the MRI measurements and the wet/dry measurements was noted.

Figure 8a shows the correlation between the water content values obtained using the LR mGRE images (LR- H_2O) and the water content values obtained using the proposed method (SRR- H_2O). The water content values using the LR images and the HR SRR images were strongly correlated. Figure 8b illustrates the advantage of using the SRR- H_2O method over using single LR mGRE images for water content mapping. The SD of the water content derived after SRR from each of the eight animals matched well with the SD of the water content of the wet/dry measurements.

Discussion

In this study, we presented a technique to achieve isotropic HR brain water content maps in rats at 9.4 T using SRR and

TABLE 1. Comparison of the Water Content Values (Mean \pm SD) Between the Ex Vivo (Wet/Dry) and In Vivo (MR) SRR-H₂O Techniques.

		FL	FR	ML	MR	CB-BS	Whole-Brain
	Wet/dry measurements [p.u.]	79.1 ± 0.4	78.9 ± 0.4	77.7 ± 0.3	77.7 ± 0.3	75.4 ± 0.5	77.5 ± 0.3
	MR measurements [p.u.] (SRR-H ₂ O)	78.9 ± 0.6	78.4 ± 0.4	77.8 ± 0.6	77.5 ± 0.2	76.2 ± 0.3	77.5 ± 0.3

 $FL = front \ left; \ FR = front \ right; \ ML = middle \ left; \ MR = middle \ right; \ CB-BS = cerebellum-brainstem.$

July 2024 169

respiration triggering. The SNR of each of the single LR acquisitions ($N_{avg} = 1$) was 50, with an acquisition time of 10 minutes. Since four averages were acquired, the SNR of the averaged LR image ($N_{avg} = 4$) was 100 (at the first TE), with an acquisition time of 40 minutes. The SNR of the first echo of the reconstructed HR mGRE image was also 100. This is expected since, as long as the anisotropy factor is equal to the improvement in resolution (as in our case), SRR is expected to improve the resolution and not the SNR. Since data were acquired in three orientations, the total measurement time using SRR was 2 hours. To generate an HR mGRE image with the same high and isotropic resolution and SNR with a direct acquisition instead of SRR, a single mGRE acquisition with $N_{avg} = 36$ would need to be acquired, requiring an acquisition time of 6 hours. Hence, the use of SRR allowed us to achieve a better trade-off between SNR and scan time as compared to averaging, and thus the derivation of high isotropic resolution water content maps. Among others, the high and isotropic resolution achieved using SRR enabled a more accurate delineation of the CSF with minimal partial volume effects, thus leading to more accurate water content values. Furthermore, the precision of the SRR-based water content, reflected by its variability over different animals, is higher than for the LR acquisitions. This is similar to a previous observation in humans,³³ and believed to be due to an averaging of the effects of physiological noise over the different orientations.

Despite unchanging the SNR, the SRR acquisition scheme and reconstruction could provide improved resolution and improved accuracy of water content values over the single-orientation scans. Further, using a TR of 3330 msec and FA of 15° could ensure a good contrast between the CSF and brain tissue, which has also been suggested by previous work.³² Since CSF voxels are rather few in the rat brain, high isotropic resolution as achieved by SRR could be helpful for obtaining accurate CSF masks. In water content mapping, the biggest problem may arise from the smoothly varying B₁ receive field inhomogeneities. In humans, this is often corrected using a correlation of T1 to proton density, ^{26,30} or, alternatively, with the method described by Ashburner et al.³⁹ However, this requires segmentation of the brain into WM, GM, and CSF classes, which is not very straightforward in animals. Hence, in this study, the N4 bias field correction algorithm was used and yielded a good B₁ inhomogeneity correction, as can be seen from the consistent values of water content with increasing penetration depth. This might be evident by the high level of accuracy obtained in different tissue regions (front, middle, and CB-BS regions) as compared to the ex vivo data. With wet/dry measurements, the three broad regions into which the brain was divided had a gradient of water content values from the anterior to the posterior areas. The differences in water content values are not surprising as different brain regions are known to have different water

content values. ^{16,24} These broad differences seen in the reference wet/dry measurements have also be accurately reflected by the MRI-based water content values, thus validating the accurate correction of the bias field. The SD of the SRR-H₂O was found to be comparable with that of the ex vivo measurements. The stability of the water content values obtained with either method is remarkable, and could reflect once more the fact that water content is tightly regulated in the healthy brain.

Gottschalk et al showed that brain water content varied with age and body weight in Wistar rats. ¹⁷ However, since all eight rats in this study were scanned between 10 and 11 weeks of age, a narrow range of brain water content values was obtained. A good correlation between ex vivo and in vivo measurements even at a whole brain level, indirectly indicates a high sensitivity of the proposed method to changes in whole-brain water content values. Although different protocols for drying the brain tissue samples exist, here we dried the samples for 42 hours at 72 °C and observed almost no change in water content after 42 hours using a basic precision scale.

Limitations

Brain masking was carried out manually. In the future, brain masking algorithms could be integrated into this method, thus making it a fully automated process. Second, for CSF masking, the threshold k was selected empirically to obtain "pure" CSF voxels and exclude voxels that were prone to partial volume effects. However, k would change with different scanner hardware and/or software, and thus an automated method of setting the threshold is desirable. Moreover, since lesions are likely to have higher than normal water content values in pathological animal models, the voxels from lesions might be falsely included in the CSF mask if an appropriate value of k is not selected. Third, the acquisition time of 2 hours is relatively long. One could choose to acquire each of the LR acquisition with N = 1, with an acquisition time of 30 minutes, leading to the same isotropic resolution of 200 µm but with half the SNR. If this is done, the regularization value should be adjusted accordingly as demonstrated in Ref. 33. Fourth, our study included only a small number of rats (N = 8). Fifth, as is noticeable, SRR-H₂O water content values of the CB-BS region are underestimated. This is possibly due to a slight overcorrection of the bias field by the N4 bias field algorithm. Since a four-channel phased array coil was used, the sensitivity in the CB-BS region was lower than in the frontal and middle regions leading to errors in the estimation of the bias field. Better bias field correction algorithms need to be developed in order to correct for the B₁ inhomogeneity accurately in regions with low coil sensitivity. Finally, T2* correction for the voxels near the ear canals was not carried out in this study. In the future, techniques like the sinc

correction could possibly be used to correct for the ${T_2}^{*}$ effects in such voxels. 40

Conclusion

An in vivo technique to achieve isotropic HR water content maps in rats using SRR and respiration triggering has been developed in this study. The MRI-derived water content values may show strong correlations with the water content values obtained using ex vivo wet/dry methods.

Acknowledgments

This work was supported by the European Union's Horizon 2020 research and innovation programme under the Marie Sklodowska-Curie grant agreement 764513. The authors would like to thank Kornadt-Beck for help with the animal approval and Claire Rick for proofreading and editing the manuscript. Open Access funding enabled and organized by Projekt DEAL.

References

- Benedikz E, Kloskowska E, Winblad B. The rat as an animal model of Alzheimer's disease. J Cell Mol Med 2009;13:1034-1042.
- Furlan R, Cuomo C, Martino G. Animal models of multiple sclerosis. In: Gordon D, Scolding NJ, editors. Neural cell transplantation: Methods and protocols. Methods in Molecular Biology™. Totowa, NJ: Humana Press; 2009. p 157-173. https://doi.org/10.1007/978-1-60327-931-4_11.
- 3. Denic A, Macura SI, Mishra P, Gamez JD, Rodriguez M, Pirko I. MRI in rodent models of brain disorders. Neurotherapeutics 2011;8:3-18.
- Xiong Y, Mahmood A, Chopp M. Animal models of traumatic brain injury. Nat Rev Neurosci 2013;14:128-142.
- Choi C-H, Stegmayr C, Shymanskaya A, et al. An in vivo multimodal feasibility study in a rat brain tumour model using flexible multinuclear MR and PET systems. EJNMMI Phys 2020;7:50.
- 6. Tofts P, editor. Quantitative MRI of the brain: Measuring changes caused by disease. Chichester: Wiley; 2003.
- Kimelberg HK. Current concepts of brain edema. Review of laboratory investigations. J Neurosurg 1995;83:1051-1059.
- O'Brien MD. Ischemic cerebral edema. A review. Stroke 1979;10: 623-628.
- Barbier EL, Liu L, Grillon E, et al. Focal brain ischemia in rat: Acute changes in brain tissue T1 reflect acute increase in brain tissue water content. NMR Biomed 2005;18:499-506.
- Lin W, Paczynski RP, Venkatesan R, et al. Quantitative regional brain water measurement with magnetic resonance imaging in a focal ischemia model. Magn Reson Med 1997;38:303-310.
- Kozler P, Riljak V, Pokorný J. Both water intoxication and osmotic BBB disruption increase brain water content in rats. Physiol Res 2013;62: S75-S80.
- Simplă V. Tissue water content and nuclear magnetic resonance in normal and tumor tissues. Cancer Res 1975;35(5):1164.
- Ferguson B, Matyszak MK, Esiri MM, Perry VH. Axonal damage in acute multiple sclerosis lesions. Brain 1997;120:393-399.
- Laule C, Vavasour IM, Moore GRW, et al. Water content and myelin water fraction in multiple sclerosis. J Neurol 2004;251:284-293.

Thomas et al.: In Vivo Measurement of Rat Brain Water Content

- Oros-Peusquens A-M, Keil F, Langen KJ, et al. Fast and accurate water content and T2* mapping in brain tumours localised with FET-PET. Nucl Instrum Methods Phys Res, Sect A 2014;734:185-190.
- Schwab M, Bauer R, Zwiener U. The distribution of normal brain water content in Wistar rats and its increase due to ischemia. Brain Res 1997; 749:82-87.
- Gottschalk A, Scafidi S, Toung TJK. Brain water as a function of age and weight in normal rats. PLoS One 2021;16:e0249384.
- Shigeno T, Brock M, Shigeno S, Fritschka E, Cervós-Navarro J. The determination of brain water content: Microgravimetry versus dryingweighing method. J Neurosurg 1982;57:99-107.
- Lin W, Venkatesan R, Gurleyik K, He YY, Powers WJ, Hsu CY. An absolute measurement of brain water content using magnetic resonance imaging in two focal cerebral ischemic rat models. J Cereb Blood Flow Metab 2000;20:37-44.
- Naessens DMP, Coolen BF, de Vos J, VanBavel E, Strijkers GJ, Bakker ENTP. Altered brain fluid management in a rat model of arterial hypertension. Fluids Barriers CNS 2020;17:41.
- Del Bigio MR, Slobodian I, Schellenberg AE, Buist RJ, Kemp-Buors TL.
 Magnetic resonance imaging indicators of blood-brain barrier and
 brain water changes in young rats with kaolin-induced hydrocephalus.
 Fluids Barriers CNS 2011;8:22.
- Neeb H, Zilles K, Shah NJ. A new method for fast quantitative mapping of absolute water content in vivo. Neuroimage 2006;31:1156-1168.
- Abbas Z, Gras V, Möllenhoff K, Oros-Peusquens A-M, Shah NJ. Quantitative water content mapping at clinically relevant field strengths: A comparative study at 1.5T and 3T. Neuroimage 2015;106:404-413.
- Oros-Peusquens A-M, Loução R, Abbas Z, et al. Rapid whole-brain protocol for quantitative water content mapping with neurobiological implications. Front Neurol 2019;10:1333.
- Meyers SM, Kolind SH, Laule C, MacKay AL. Measuring water content using T2 relaxation at 3T: Phantom validations and simulations. Magn Reson Imaging 2016;34:246-251.
- Volz S, Nöth U, Jurcoane A, Ziemann U, Hattingen E, Deichmann R. Quantitative proton density mapping: Correcting the receiver sensitivity bias via pseudo proton densities. Neuroimage 2012;63:540-552.
- Venkatesan R, Lin W, Gurleyik K, et al. Absolute measurements of water content using magnetic resonance imaging: Preliminary findings in an in vivo focal ischemic rat model. Magn Reson Med 2000;43: 146-150.
- Schwarcz A, Berente Z, Ősz E, Dóczi T. In vivo water quantification in mouse brain at 9.4 Tesla in a vasogenic edema model. Magn Reson Med 2001;46:1246-1249.
- Fatouros PP, Marmarou A, Kraft KA, Inao S, Schwarz FP. In vivo brain water determination by T1 measurements: Effect of total water content, hydration fraction, and field strength. Magn Reson Med 1991;17: 402-413
- Abbas Z, Gras V, Möllenhoff K, Keil F, Oros-Peusquens A-M, Shah NJ. Analysis of proton-density bias corrections based on T₁ measurement for robust quantification of water content in the brain at 3 Tesla: Quantitative water content mapping at 3T. Magn Reson Med 2014;72:1735-1745.
- Plenge E, Poot DHJ, Bernsen M, et al. Super-resolution methods in MRI: Can they improve the trade-off between resolution, signalto-noise ratio, and acquisition time? Magn Reson Med 2012;68:1983-1993.
- D. C. Thomas, A.-M. Oros-Peusquens, D. Poot, N. J. Shah, Isotropic water content mapping employing super-resolution reconstruction with acquisition in three orthogonal orientations. In: 2021 ISMRM & SMRT Annual Meeting & Exhibition 15–20 May 2021; 2021.
- Thomas DC, Oros-Peusquens A-M, Poot D, Shah NJ. Whole-brain water content mapping using super-resolution reconstruction with MRI acquisition in 3 orthogonal orientations. Magn Reson Med 2022;88: 2117-2130.

July 2024 171

Journal of Magnetic Resonance Imaging

- Felder J, Celik AA, Choi C-H, Schwan S, Shah NJ. 9.4 T small animal MRI using clinical components for direct translational studies. J Transl Med 2017;15:264.
- Poot DHJ, Van Meir V, Sijbers J. General and efficient super-resolution method for multi-slice MRI. In: Jiang T, Navab N, Pluim JPW, Viergever MA, editors. Medical image computing and computerassisted intervention – MICCAI 2010. Berlin: Springer Berlin Heidelberg; 2010. p 615-622.
- Yushkevich PA, Piven J, Hazlett HC, et al. User-guided 3D active contour segmentation of anatomical structures: Significantly improved efficiency and reliability. Neuroimage 2006;31:1116-1128.
- Tustison NJ, Avants BB, Cook PA, et al. N4ITK: Improved N3 bias correction. IEEE Trans Med Imaging 2010;29:1310-1320.
- Gerriets T, Stolz E, Walberer M, et al. Noninvasive quantification of brain edema and the space-occupying effect in rat stroke models using magnetic resonance imaging. Stroke 2004;35:566-571.
- Ashburner J, Friston KJ. Unified segmentation. Neuroimage 2005;26: 839-851.
- Reichenbach JR, Venkatesan R, Yablonskiy DA, Thompson MR, Lai S, Haacke EM. Theory and application of static field inhomogeneity effects in gradient-echo imaging. J Magn Reson Imaging 1997;7: 266-279.